Electronic Materials Letters, Vol. 1, No. 2 (2005), pp. 141-147

Nanosize Control of Final Products from Sol-Gel Reactions for Optical Waveguides

Se Yun Kim and Jeung Ku Kang*

Department of Materials Science and Engineering, Korea Advanced Institute of Science and Technology, Daejeon 305-701, Korea

We determined the mechanism and the nanosize products of a sol-gel reaction with diphenylsilanediol (DPD) and 3-methacryloxypropyltrimethoxysilane (MEMO) precursors for synthesizing an optical waveguide material. From the first-principles calculation, we found that diphenyldimethoxysilane (DPDM) and 3-methacryloxypropylmethoxysilanediol (MEMDO) are generated through the first two steps, and we also determined that the reaction pathway could be modified by the presence of H_2O released from a catalyst such as $Ba(OH)_2 \cdot H_2O$. In the final step, condensation between a MEMDO hydroxyl and a DPDM methoxy occurs, generating a DPDM-MEMDO dimer and CH_3OH molecule as products. In a similar fashion, the DPDM of the DPDM-MEMDO dimer can condense with the MEMDO of another DPDM-MEMDO dimer to increase the chain, but its reaction rate of 2.8×10^{-11} per second is predicted to be about five times smaller than that between DPDM and MEMDO. This implies that the reaction rate becomes smaller for larger nanostructures.

Keywords: optical waveguides, density functional theory, sol-gel reaction, organic-inorganic hybrid materials, catalyst

I. INTRODUCTION

There is currently great interest in designing ideal waveguide materials for optical applications. Conventionally, waveguides have been made of inorganic glasses[1,2] and organic polymers[3,4]. However, it is quite challenging to reduce optical losses and to make waveguides that have good adhesion on various substrates, high thermal stability, and low processing temperatures. Recently, hybrid materials[5-7] that have both organic and inorganic components have been proposed as good candidates to satisfy simultaneously the ideal properties and processing conditions. In addition, synthesizing hybrid materials with nanometer scale sizes facilitates the development of fine nanostructures and waveguides with homogeneous properties.

Hydrolytic and non-hydrolytic processes have both been proposed for the production of hybrid materials. However, synthesizing hybrid materials by hydrolytic processes results in more optical losses than when non-hydrolytic processes[8-11] are used, because hydrolytic processes[12,13] generally generate more unwanted hydroxyls that are sensitive to vibration excitations. Also, depending on the nature of the interface between the organic and inorganic elements, the hybrid materials can be classified into two different groups [14,15]. In one group, organic and inorganic components are linked up through van der Waals or hydrogen bonding, while in the other group, the network is formed through covalent or ionic bonding. The non-hydrolytic synthesis of hybrid materials consists of a two-step process[16]. In the first step, the precursors are linked up to produce siloxane (-Si-O-Si-) bridges, while the second step involves cross-linking between the organic side chains of inorganic structures in a three-dimensional network by ultra-violet (UV) light. Buestrich *et al.*[7] and Houbertz *et al.*[17,18] synthesized a hybrid material on the sol-gel reactions[19] using diphenylsilanediol (DPD) and 3-methacryloxypropyltrimethoxysilane (MEMO) precursors. Combining DPD that had OH groups for non-hydrolytic processes with the MEMO enabled the resulting materials to be patterned by UV, which created a good precursor system. The IR study by Buestrich *et al.*[7] shows that there is no SiO-H stretching mode (3600-3200 cm^{-1}) in their synthesized hybrid material, so there are low scattering losses (0.3 dB/cm at 1320 nm and 0.6 dB/cm at 1550 nm). This hybrid material also demonstrates good adhesion on a silicon substrate, and has a relatively low processing temperature of 150 °C. However, detailed thermodynamic and kinetic parameters for the intermediate nanostructures likely to be produced from the reactions using DPD and MEMO precursors have not yet been reported. Also, a considerable amount of ambiguity still remains regarding whether or not the final products from the

*Corresponding author: jeungku@kaist.ac.kr

sol-gel reaction would be in nanometer scale sizes.

Here, we use first-principles calculation[20-22] and small angle neutron scattering (SANS) methods to determine the mechanisms and intermediate nanostructures for the sol-gel processes using DPD and MEMO precursors. First, we investigate three condensation reactions: between two DPDs, between one DPD and one MEMO, and between two MEMOs. Also, the switching reaction between one DPD hydroxyl and one MEMO methoxy is explored; this reaction generates diphenylmethoxysilanol (DPM) and 3-methacryloxypropyldimethoxysilanol (MEDO) as products. Then, the catalytic effects caused by releasing H_2O from a catalyst such as $Ba(OH)_2 \cdot H_2O$ are additionally investigated to determine if they play an important role in reducing the reaction barrier, as has been suggested in previous studies[23-25]. Moreover, the reactions by DPM and MEDO molecules are explored, as are the reactions by the diphenyldimethoxysilane (DPDM) and 3-methacryloxypropylmethoxysilanediol (MEMDO) molecules, and the reactions by the dimer (DPDM-MEMDO) molecules. Lastly, the sizes of the final products are determined based on experimental SANS measurements and theoretical predictions.

These results are reported and discussed in Section 3. Section 2 provides some details about the calculations while Section 4 summarizes our results.

2. ANALYSIS DETAILS

All calculations are performed using the self-consistent B3LYP[20] and KMLYP[21] density functional theories and the QCISD[22] level of theory. The B3LYP was shown to predict geometries and thermochemical data more accurately than other generalized gradient approximation (GGA) [26-30] and local density approximation (LDA) [31,32] techniques, while the KMLYP was proven to be more accurate in predicting transition state barriers[21,33,34] than other DFT methods.

The electronic wave function is expanded using the 6-31G valence double-zeta[35] basis set and the 6-311+G(d,p) valence diffuse triple-zeta plus polarization[35] basis set. In this study, the full optimizations of all geometry parameters for reactants, transition states, and products are performed at the B3LYP/6-31G level of theory and then the enthalpies of reactions and transition state barriers are obtained using the KMLYP/6-311+G(d,p) single-point energies determined at the B3LYP geometries. All the calculations here are performed with Gaussian03[36].

We use DPD and MEMO precursors to make siloxane bridges. The DPD consists of one silicon atom, two hydroxyls, and two phenyl groups. The valence orbitals for the silicon atom are sp^3 hybridized and they bond to two phenyl and two hydroxyl fragments, as shown in Fig. 1(a). Our predicted DPD Si-OH bond length of 1.64 Å is found to be in close agreement with the experimental values of 1.63~1.64 Å [37,38]. In addition, the DPD Si-phenyl bond length of 1.89 Å is calculated to be consistent with the QCISD value of 1.90 Å . The MEMO molecule has one 3-methacryloxypropyl group and three methoxy groups around the silicon atom, as described in Fig. 1(b). For all the possible sol-gel processes that use the DPD and MEMO precursors system, the Si-OH fragments of the DPD and the $Si-OCH_3$ fragments of the MEMO are the active groups that form the siloxane bridge (-Si-O-Si-), thereby releasing the H_2O or CH_3OH as the byproduct.

3. RESULTS AND DISCUSSION

3.1. Reaction mechanism and final nanostructures

By computing the partition functions for the reactants and the transition state, the reaction rate k^{TST} of the canonical rate equation[39] is determined by

$$k^{TST} = \Gamma(T)\frac{k_B T}{h}\frac{Q_{TS}}{Q_A Q_B} exp\left(\frac{-\Delta E_0}{k_B T}\right) \quad (1)$$

where $\Gamma(T)$ is the thermal tunneling coefficient[21], k_B is the Boltzmann constant, h is the Plank constant, Q_{TS} is the partition function for the transition state, Q_A and Q_B are the partition functions for the reactants A and B, and ΔE_0 is the barrier height. We determine the sequence of the reactions by comparing the calculated reaction rates.

There are three plausible cases for condensation in the first step of the sequence: 1) reactions between two DPDs, 2) reactions between one DPD and one MEMO, and 3) reactions between two MEMOs. In the first case, a DPD hydroxyl attacks another DPD hydroxyl and then proceeds through the four-centered transition state, as shown in Fig. 2a. The predicted barrier for this case is 14.9 kcal/mol. The

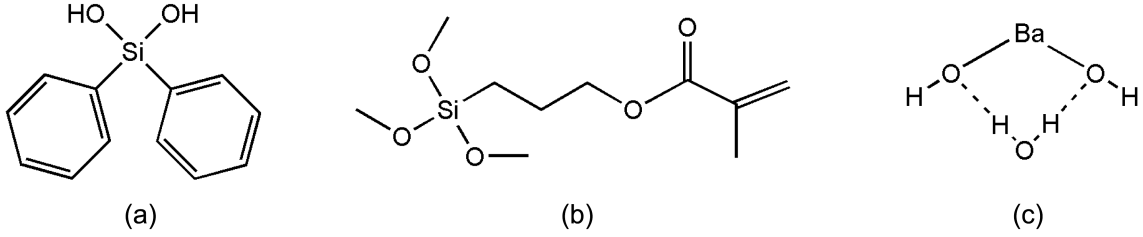

Fig. 1. Reactants and catalyst: (a) DPD(diphenylsilanediol) and (b) MEMO (3-methacryloxypropyltrimethoxysilane), and (c) $Ba(OH)_2 \cdot H_2O$.

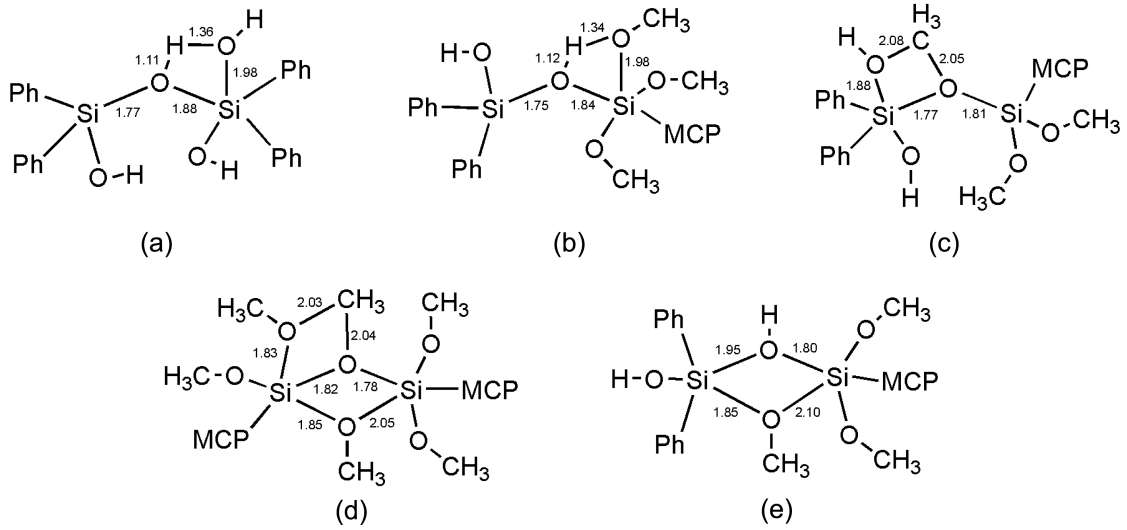

Fig. 2. B3LYP/6-31G transition state geometries for condensations (a) between a DPD hydroxyl on a DPD hydroxyl, (b) between a DPD hydroxyl on a MEMO methoxy, (c) between a MEMO methoxy on a DPD hydroxyl, and (d) between a MEMO methoxy on a MEMO methoxy, as well as for the switching reaction between (e) a DPD hydroxyl and a MEMO methoxy. Ph and MCP indicate phenyl and methacryloxypropyl groups, respectively. Bond lengths are in units of Å.

second condensation case can occur through one of two different reaction pathways; either a DPD hydroxyl attacks a MEMO methoxy (see Fig. 2b), or a MEMO methoxy attacks a DPD hydroxyl (see Fig. 2c). However, it is preferable if the former pathway is used, as an attack initiated by a DPD results in a smaller barrier (15.1 kcal/mol), which is more favorable than another. Figure. 2d describes the condensation reaction between two MEMOs, but its predicted barrier of 69.3 kcal/mol is considerably higher than in the first two cases. Our calculations indicate that switching between a DPD hydroxyl and a MEMO methoxy is most likely to occur at the first reaction step, as the switching reaction is predicted to have a rate of 6.80×10^{-6} per second at 300 K, which is much larger than the rates of 3.77×10^{-9} and 1.81×10^{-10} per second for condensations between the two DPDs and the one DPD and one MEMO, respectively. For the switching reaction, it is found that the concerted attacks of a DPD hydroxyl on a MEMO silicon and of a MEMO methoxy on a DPD silicon will generate DPM (a DPD hydroxyl substituted with one methoxy) and MEDO (a MEMO methoxy substituted with one hydroxyl) as products. At the transition state, the DPD Si-OH bond (1.95 Å) is significantly broken while a MEMO Si-OH bond is being formed, as shown in Fig. 2e. Simultaneously, the Si-OCH_3 bond begins to form on the DPD side while the MEMO Si-OCH_3 bond length of 2.10 Å indicates a considerable amount of breakage in the bond.

There are ten possible cases for condensation in the second reaction step. These possible reactions are: 1) between two DPM hydroxyls, 2) between one DPM hydroxyl and one DPM methoxy, 3) between two DPM methoxys, 4) between one DPM hydroxyl and one MEDO hydroxyl, 5) between

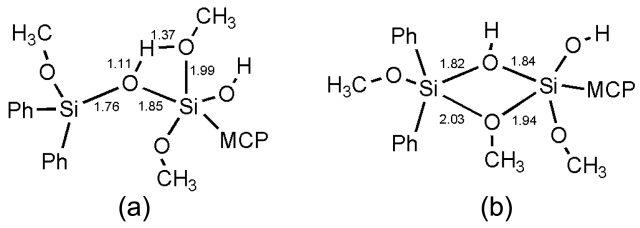

Fig. 3. B3LYP/6-31G transition state geometries for (a) condensation between a DPM hydroxyl and a MEDO methoxy, and (b) switching between a DPM hydroxyl and a MEDO methoxy. Ph and MCP indicate phenyl and methacryloxypropyl groups, respectively. Bond lengths are in units of Å.

one DPM methoxy and one MEDO hydroxyl, 6) between one DPM hydroxyl and one MEDO methoxy, 7) between one DPM methoxy and one MEDO methoxy, 8) between two MEDO hydroxyls, 9) between one MEDO hydroxyl and one MEDO methoxy, and 10) between two MEDO methoxys. All calculated transition barriers and enthalpies are summarized in Table 1. Among these reactions, the attack of a DPM hydroxyl on a MEDO methoxy is found to have the largest rate, 1.12×10^{-8} per second; the transition state structure is shown in Fig. 3a. However, it is determined that the switching reaction between a DPM hydroxyl and a MEDO methoxy, generating DPDM and MEMDO as products, will have a much larger rate, 4.61×10^{-7} per second, than the rates for condensation. In this respect, the switching reaction is determined as the fastest process at the second reaction step. The transition state for the switching reaction involves several simultaneous bond breakings and formations: 1) the breaking of a DPM Si-OH bond with an elongated bond length of 1.82 Å, 2) the formation of a 1.84 Å Si-OH bond

between a DPM hydroxyl and a MEDO silicon, 3) the breaking of a Si-OCH_3 bond with an elongated 1.94 Å bond on the MEDO side, and 4) the formation of a 2.03 Å Si-OCH_3 on the DPM side, as shown in Fig. 3b.

DPDM and MEMDO are produced during the switching reaction at the second reaction step. There are three possible condensation reactions that can occur at this step. First, a MEMDO hydroxyl can attack a DPDM methoxy. This possibility is shown in Fig. 4a,where the transition barrier is 14.0 kcal/mol. Figure 4b and 4c show the other two possibilities: condensation reactions between two MEMDO hydroxyls and between one MEMDO hydroxyl and one MEMDO

Table 1. KMLYP/6-311+G(d,p)//B3LYP/6-31G transition state barriers and enthalpies for sol-gel processes using DPD and MEMO precursors. Energies are in units of kcal/mol.

Sequence	Reaction	Barrier	Enthalpy
Step I	· Condensation Reaction		
	DPD OH+DPD OH → DPD-DPD+H_2O	14.9	-9.1
	DPD OH+MEMO OCH_3 → DPD-MEMO+CH_3OH [a]	15.1	-8.4
	DPD OH+MEMO OCH_3 → DPD-MEMO+CH_3OH [b]	73.1	-8.4
	MEMO OCH_3+MEMO OCH_3 → MEMO-MEMO+$(CH_3)_2O$	69.3	-12.7
	· Switching Reaction		
	DPD OH+MEMO OCH_3 → DPM+MEDO	6.9	-0.4
Step II	· Condensation Reaction		
	DPM OH+DPM OH → DPM-DPM(I)+H_2O	18.5	-9.7
	DPM OH+DPM OCH_3 → DPM-DPM(II)+CH_3OH [c]	16.3	-8.3
	DPM OH+DPM OCH_3 → DPM-DPM(II)+CH_3OH [d]	68.5	-8.3
	DPM OCH_3+DPM OCH_3 → DPM-DPM (III)+$(CH_3)_2O$	69.5	-11.9
	DPM OH+MEDO OH → DPM-MEDO(I)+H_2O [e]	15.8	-9.4
	DPM OH+MEDO OH → DPM-MEDO(I)+H_2O [f]	17.7	-9.4
	DPM OCH_3+MEDO OH → DPM-MEDO(II)+CH_3OH [g]	16.2	-8.0
	DPM OCH_3+MEDO OH → DPM-MEDO(II)+CH_3OH [h]	64.6	-8.0
	DPM OH+MEDO OCH_3 → DPM-MEDO(III)+CH_3OH [i]	12.1	-8.2
	DPM OH+MEDO OCH_3 → DPM-MEDO(III)+CH_3OH [j]	65.6	-8.2
	DPM OCH_3+MEDO OCH_3 → DPM-MEDO(IV)+$(CH_3)_2O$ [k]	59.9	-11.7
	DPM OCH_3+MEDO OCH_3 → DPM-MEDO(IV)+$(CH_3)_2O$ [l]	73.1	-11.7
	MEDO OH+MEDO OH → MEDO-MEDO(I)+H_2O	19.5	-9.0
	MEDO OH+MEDO OCH_3 → MEDO-MEDO(II)+CH_3OH [m]	16.8	-9.3
	MEDO OH+MEDO OCH_3 → MEDO-MEDO(II)+CH_3OH [n]	71.8	-9.3
	MEDO OCH_3+MEDO OCH_3 → MEDO-MEDO(III)+$(CH_3)_2O$	68.2	-13.0
	· Switching Reaction	8.5	-0.60
	DPM OH+MEDO OCH_3 → DPDM +MEMDO		
Step III	· Condensation Reaction		
	DPDM OCH_3+MEMDO OH → DPDM-MEMDO+CH_3OH	14.0	-7.6
	MEMDO OH+MEMDO OH → MEMDO-MEMDO(I)+H_2O	18.7	-9.1
	MEMDO OH+MEMDO OCH_3 → MEMDO-MEMDO(II)+CH_3OH	19.8	-8.3

[a]DPD OH attack, [b]MEMO OCH_3 attack, [c]DPM OH attack, [d]DPM OCH_3 attack, [e]DPM OH attack, [f]MEDO OH attack, [g]MEDO OH attack, [h]DPM OCH_3 attack, [i]DPM OH attack, [j]MEDO OCH_3 attack, [k]DPM OCH_3 attack, [l]MEDO OCH_3 attack, [m]MEDO OH attack, [n]MEDO OCH_3 attack.

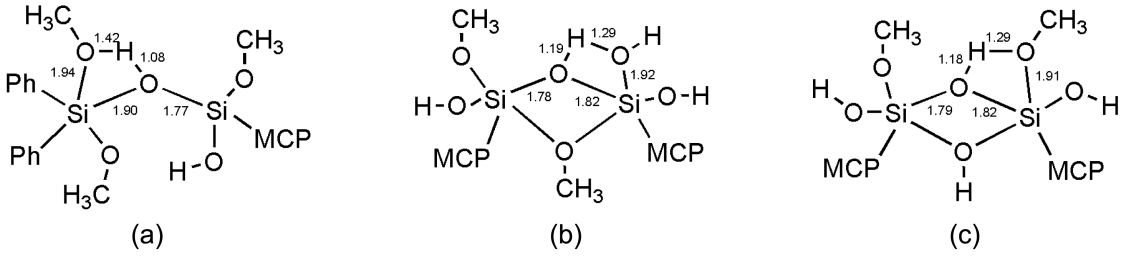

Fig. 4. B3LYP/6-31G transition state geometries for condensations (a) between a DPDM methoxy and a MEMDO hydroxyl, (b) between two MEMDO hydroxyls, and (c) between a MEMDO hydroxyl and a MEMDO methoxy. Ph and MCP indicate phenyl and methacryloxypropyl groups, respectively. Bond lengths are in units of Å.

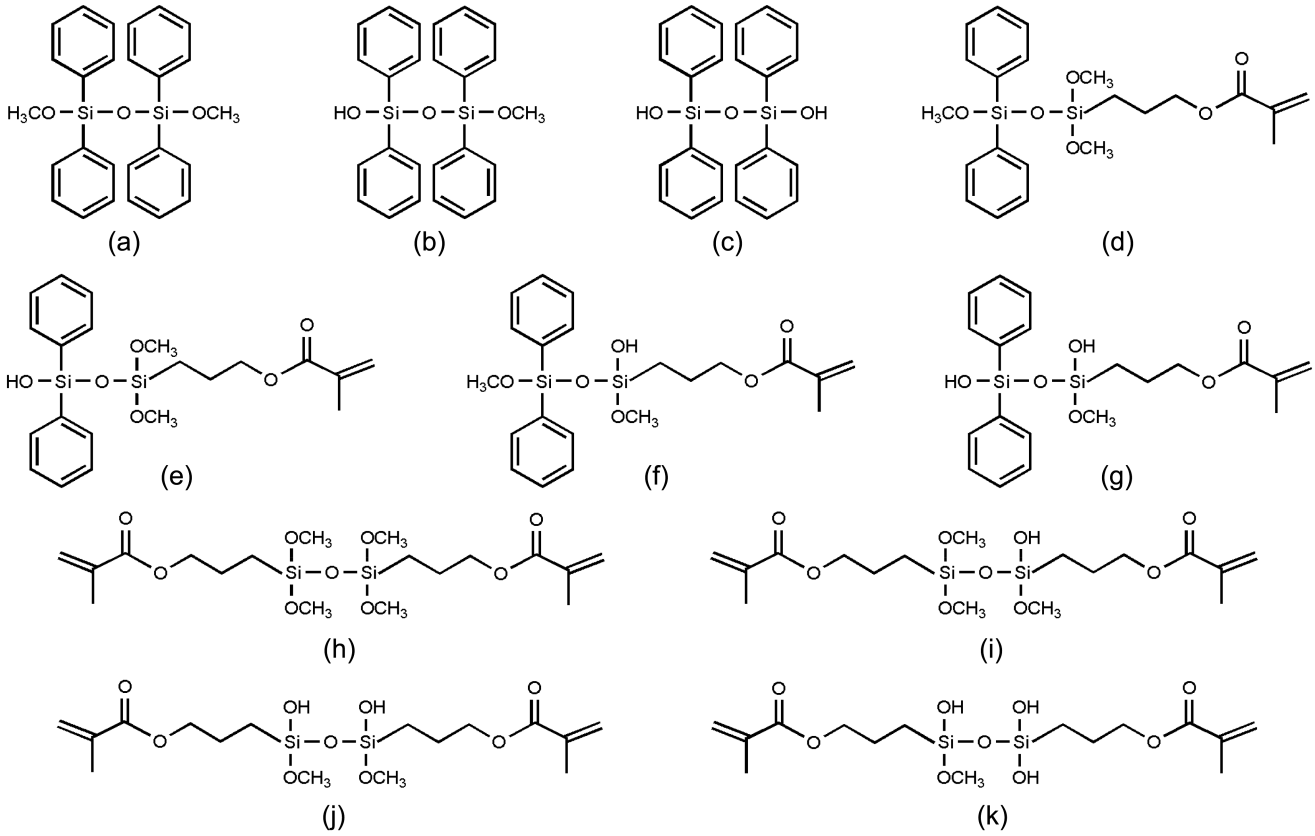

Fig. 5. Products for condensations between (a) two DPM hydroxyls, (b) a DPM hydroxyl and a DPM methoxy, (c) two DPM methoxys (or two DPD hydroxyls), (d) one DPM hydroxyl and one MEDO hydroxyl, (e) one DPM methoxy and one MEDO hydroxyl (or one DPD hydroxyl and one MEMO methoxy), (f) one DPM hydroxyl and one MEDO methoxy (or one DPDM methoxy and one MEMDO hydroxyl), (g) one DPM methoxy and one MEDO methoxy, (h) two MEDO hydroxyls (or two MEMO methoxys), (i) one MEDO hydroxyl and one MEDO methoxy, (j) two MEDO methoxys (or two MEMDO hydroxyls), and (k) one MEMDO hydroxyl and one MEMDO methoxy.

methoxy, respectively, with barriers of 18.7 kcal/mol and 19.8 kcal/mol. We find that the first reaction, in which there is condensation between one DPDM methoxy and one MEMDO hydroxyl, has the largest reaction rate, 1.22×10^{-10} per second.Therefore, at the third reaction step, the process for producing the "DPDM-MEMDO" dimer that is shown in Fig. 5f is considered to be the most probable. The dimer can also be increased by condensation between the methoxy of a dimer DPDM site and the hydroxyl of a dimer MEMDO site, but its reaction is determined to have a smaller rate, 2.76×10^{-11} per second, than the case in which the reaction occurs between a DPDM methoxy and a MEMDO hydroxyl. Meanwhile, however, this rate is found to be slightly larger than the 1.17×10^{-11} per second rate for condensation between the hydroxyl of a dimer MEMDO site and the methoxy of a dimer MEMDO site. Here, it should be noted that the reaction rate is smaller for the larger nanostructures, which might be due to the increased geometry hindrance. Additionally, our SANS measurements determined that the final products from the sol-gel reaction are mostly in nanometer scale sizes of 1.76 to 2.36 nm, which compare to the value of 2.01 nm determined on the elongated product by three dimers. The experimental size of the products is determined from the R_g (radius of gyration) of the products measured by SANS. The products of the reaction between DPD (50 mol %) and MEMO (50 mol %) are solvated to acetone-d_6 in 10 wt % to obtain accurate SANS results. In this condition, the R_g of the products is 0.68 nm. When the structure of the particle is spherical, the radius of the particle is $R = \sqrt{\frac{5}{3}} R_g$, while the length of a rod-like particle is $L = \sqrt{12} R_g$. Consequently, the experimentally predicted size of the products is in the range of 1.76 nm to 2.36 nm.

3.2. H_2O effects on the sol-gel reaction

H_2O can be released from the catalyst. The enthalpy of H_2O dissociation from the catalyst of $Ba(OH)_2 \cdot H_2O$ is calculated to be endothermic by 3.8 kcal/mol while that from $Sr(OH)_2 \cdot H_2O$ and $Ca(OH)_2 \cdot H_2O$ is endothermic by 3.2 kcal/mol and 2.5 kcal/mol, respectively. Figure 6a describes a concerted H_2O attack on the hydroxyl fragments of two DPDs in which a six-centered structure is formed, involving

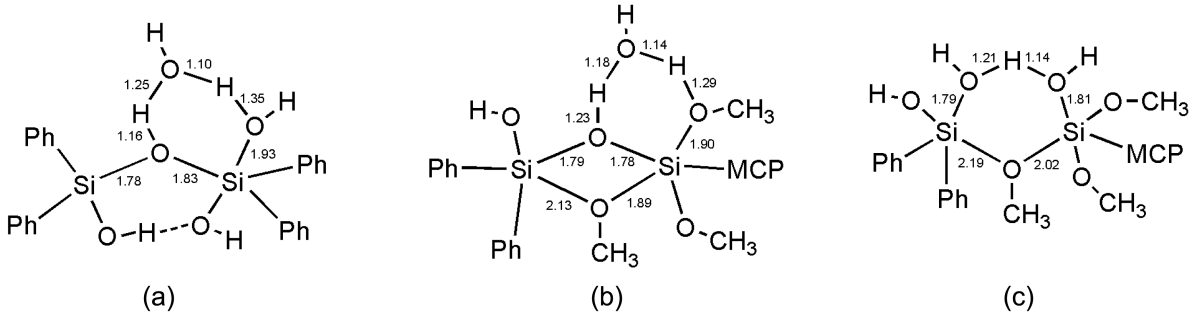

Fig. 6. Catalytic effects of the H_2O on transition states for (a) condensation between two DPDs, (b) condensation between a DPD hydroxyl and a MEMO methoxy, and (c) switching between a DPD hydroxyl and a MEMO methoxy. Ph and MCP indicate the phenyl group and methacryloxypropyl group, respectively. Bond lengths are in units of Å, where the B3LYP/6-31G geometries are used.

the transfer of one H atom from the H_2O to the DPD hydroxyl, the bond dissociation of a Si-O bond to generate one H_2O molecule, the transfer of one H atom from the DPD OH to the attacking H_2O, and the formation of a Si-O-Si bond. It should be noted that the H_2O participates in this reaction as a catalyst donating one hydrogen atom to the DPD hydroxyl and simultaneously accepting one hydrogen atom from the other DPD hydroxyl.The predicted barrier for this reaction is 16.9 kcal/mol with respect to an intermediate water complex formed from two DPD molecules, and this reaction is determined to be exothermic by 3.3 kcal/mol. Consequently, its predicted barrier and exothermic enthalpy indicate that the presence of the H_2O included in the catalyst can reduce significantly the condensation rate between the two DPDs. Before making a transition state structure, the H_2O and two DPD molecules form a water-mediated structure with a high exothermic enthalpy of 20.0 kcal/mol due to the three hydrogen bonds that exist between one hydrogen atom of the H_2O and the oxygen atom of a DPD hydroxyl, between one H atom of another DPD hydroxyl and the oxygen atom of the H_2O molecule, and between the hydrogen atom of one DPD and the oxygen atom of another DPD.

A concerted attack of DPD on MEMO in the presence of H_2O is also described in Fig. 6b, where the transition state is a six-centered ring structure that is similar to the previous one. We obtain a transition state barrier of 12.5 kcal/mol and find that this process is exothermic by 4.9 kcal/mol. The decreased barrier indicates that the presence of the catalyst can increase the condensation rate between one DPD and one MEMO, which is the opposite result of that obtained in the reaction between two DPDs.

The H_2O effect on the switching reaction between DPD and MEMO is also explored. The transition state of this reaction is also based on a six-centered ring structure, as shown in Fig. 6c. The transition barrier for this case is 30.5 kcal/mol, which is higher than for cases of DPD with DPD and of DPD with MEMO. Consequently, this result indicates that the final nanostructure could be modified by the presence of H_2O because the H_2O released from the catalyst plays an important role in changing reaction pathways to modify the resulting product.

4. CONCLUSIONS

Making hybrid materials from a sol-gel reaction with nanometer scale sizes is one of today's vital research areas because the nanosizes of the resulting hybrid materials can be used to make the fine nanostructures of optical waveguides and to obtain homogeneous properties within a waveguide. The first-principles calculation and experimental SANS measurement methods have been used to investigate the mechanism and the nanosize products of the sol-gel reaction using DPD and MEMO precursors. To determine the size of the products resulting from the sol-gel reaction, first, we have explored the reaction mechanism by comparing the rates of all the possible reactions at each step. It has been found that the switching reaction between a DPD hydroxyl and a MEMO methoxy, which has a kinetic reaction rate of 6.80×10^{-6} per second at room temperature and generates one DPM and one MEDO as products, is the fastest process at the first reaction step. On the other hand, it has been determined that the reaction pathway can be modified by the presence of a catalyst such as $Ba(OH)_2 \cdot H_2O$, since the H_2O released from the catalyst changes the reaction barrier. In the second reaction step, we have also found that the switching reaction between the DPM hydroxyl and the MEDO methoxy that forms DPDM and MEMDO is the most favorable as it has a reaction rate of 4.61×10^{-7} per second. Next, the condensation between a methoxy of DPDM and a hydroxyl of MEMDO, with a reaction rate of 1.22×10^{-10} per second, has been determined as the most favorable at the third reaction step. This reaction generates the "DPDM-MEMDO" dimer and additional growth has been found to occur by condensation between a methoxy of the dimer in the DPDM site and a hydroxyl of the dimer in the MEMDO site, with a reaction rate of 2.76×10^{-11} per second. In addition, our SANS measurements have shown that the final products for the sol-gel reaction are in nanometer scale sizes of 1.76 to

2.36 nm, which compare to the 2.01 nm size of the elongated structure by three dimers. This result implies that the reaction rate on the larger nanostructures becomes insignificant.

ACKNOWLEDGEMENTS

Computational resources at the Materials and Process Simulation Center (MSC) at the California Institute of Technology and at the Korea Advanced Institute of Science and Technology have been supported by grants from NSF-MRI, ARO-DURIP, and by a SUR grant from IBM.

REFERENCES

1. M. Okoshi, M. Kuramatsu, and N. Inoue, *Appl. Phys. Lett.* **81**, 789 **(**2002).
2. L. Zhang, W. Xie, Y. Wu, H. Xing, A. Li, W. Zheng, and Y. Zhang, *Opt. Mater.* **22**, 283 (2003).
3. J. S. Koo, P. G. R. Smith, R. B. Williams, C. Riziotis, and M. C. Grossel, *Opt. Mater.* **23**, 583 (2003).
4. M. Hikita, R. Yoshimura, M. Usui, S. Tomaru, and S. Imamura, *Thin Solid Films* **331**, 303 (1998).
5. P. Coudray, J. Chisham, A. Malek-Tabrizi, C.-Y. Li, M. P. Andrews, N. Peyghambarian, and S. I. Najafi, *Optics Communications* **128**, 19 (1996).
6. S. I. Najafi, T. Touam, R. Sara, M. P. Andrews, and M. A. Fardad, *J. Lightwave Technol.* **16**, 1640 (1998).
7. R. Buestrich, F. Kahlenberg, M. Popall, P. Dannberg, R. Müller-Fiedler, and O. Rösch, *J. Sol-Gel Sci. Technol.* **20**, 181 (2001).
8. J. N. Hay and H. M. Raval, *Chem. Mater.* **13**, 3396 (2001).
9. L. Bourget, R. J. P. Corriu, D. Leclercq, P. H. Mutin, and A. Vioux, *J. Non-Cryst. Solids* **242**, 81 (1998).
10. L. Bourget, D. Leclercq, and A. Vioux, *J. Sol-Gel Sci. Technol.* **14**, 137 (1999).
11. J. N. Hay, D. Porter, and H. M. Raval, *J. Mater. Chem.* **10**, 1811 (2000).
12. D. A. Loy and K. J. Shea, *Chem. Rev.* **95**, 1431 (1995).
13. J. E. Mark, *Polym. Eng. Sci.* **36**, 2905 (1996).
14. K. H. Haas, *Adv. Eng. Mater.* **2**, 571 (2000).
15. C. Sanchez and F. Ribot, *New. J. Chem.* **18**, 1007 (1994).
16. P. Judeinstein and C. Sanchez, *J. Mater. Chem.* **6**, 511 (1996).
17. R. Houbertz, L. Fröhlich, M. Popall, U. Streppel, P. Dannberg, A. Bräuer, J. Serbin, and B. N. Chichkov, *Adv. Eng. Mater.* **5**, 551 (2003).
18. R. Houbertz, G. Domann, C. Cronauer, A. Schmitt, H. Martin, J.-U. Park, L. Fröhlich, R. Buestrich, M. Popall, U. Streppel, P. Dannberg, C. Wächter, and A. Bräuer, *Thin Solid Films* **442**, 194 (2003).
19. L. L. Hench and J. K. West, *Chem. Rev.* **90**, 33 (1990).
20. A. D. Becke, *J. Chem. Phys.* **98**, 5648 (1993).
21. J. K. Kang and C. B. Musgrave, *J. Chem. Phys.* **115**, 11040 (2001).
22. J. A. Pople, M. Head-Gordon, and K. Raghavachari, *J. Chem. Phys.* **87**, 5968 (1987).
23. J. K. Kang and C. B. Musgrave, *J. Chem. Phys.* **116**, 275 (2002).
24. R. McIntosh, T. S. Kuan, and E. Defresart, *J. Electron. Mater.* **21**, 57 (1992).
25. S. H. Garofalini, *J. Non-Cryst. Solids* **120**, 1 (1990).
26. A. D. Becke, *J. Chem. Phys.* **85**, 7184 (1986).
27. J. P. Perdew, *Phys. Rev. B* **33**, 8822 (1986).
28. A. D. Becke, *Phys. Rev. A* **38**, 3098 (1988).
29. P. M. W. Gill, *Mol. Phys.* **89**, 433 (1996).
30. J. P. Perdew, K. Burke, and M. Ernzerhof, *Phys. Rev. Lett.* **77**, 3865 (1996).
31. J. C. Slater, *Quantum Theory of Molecular and Solids: The Self-Consistent Field for Molecular and Solids* **4**, McGraw-Hill, New York (1974).
32. S. H. Vosko, L. Wilk, and M. Nusair, *Can. J. Phys.* **58**, 1200 (1980).
33. J. K. Kang and C. B. Musgrave, *J. Appl. Phys.* **91**, 3408 (2002).
34. J. K. Kang and C. B. Musgrave, *J. Chem. Phys.* **116**, 9907 (2002).
35. A. D. McLean and G. S. Chandler, *J. Chem. Phys.* **72**, 5639 (1980); R. Ditchfield, W. J. Hehre, and J. A. Pople, *J. Chem. Phys.* **54**, 724 (1971); M. J. Frisch, J. A. Pople, and J. S. Binkley, *J. Chem. Phys.* **80**, 3265 (1984).
36. *Gaussian 03*; Gaussian, Inc.: Pittsburgh, PA, 2003.
37. J. K. Fawcett, N. Camerman, and A. Camerman, *Can. J. Chem.* **55**, 3631 (1977).
38. L. Párkányi and G. Bocelli, *Cryst. Struct. Commun.* **7**, 335 (1978).
39. K. J. Laidler, *Chemical Kinetics* Chapter 3, McGraw-Hill, New York (1950).